ELSEVIER

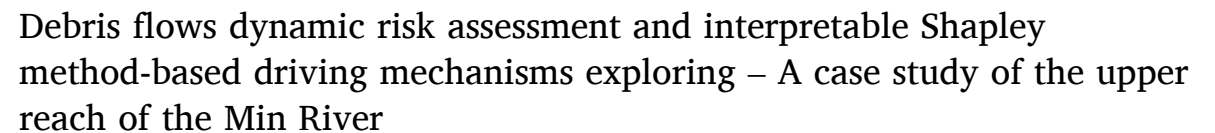
Contents lists available at ScienceDirect

Ecological Indicators

journal homepage: www.elsevier.com/locate/ecolind



Original Articles





- ^a Faculty of Geosciences and Engineering, Southwest Jiaotong University, Chengdu 611756, China
- b Institute for Disaster Management and Reconstruction, Sichuan University-Hongkong Polytechnic University, Chengdu 610207, China
- ^c School of Geography and Planning, Sun Yat-sen University, Guangzhou 510275, China

ARTICLE INFO

Keywords: Debris flows Risk assessment Machine learning Model interpretability Indicators contribution

ABSTRACT

Debris flow is one of the most devastating natural hazards. Identifying the dynamic changes and driving factors of debris flow risk can enhance hazard mitigation and prevention. It is not clear what factors can mostly lead to debris flow risk change in mountainous areas, particularly some of these areas in the context of intense earth-quakes, rapid urbanization, and climate change. To address these questions, an ensemble learning model was constructed to estimate the debris flow risk of the baseline period (2000) and the current period (2020) in the upper reach of the Min River. The study found that the areas with extremely high debris flow risk decreased by 18.57%, while the areas with moderate and high risk levels increased by 8% and 14% respectively. With this trend of overall risk increasing, the population and buildings affected by extremely high debris flow risk have increased by 20% and 30% respectively. Based on the interpretable learning model of SHAP (The Shapley Additive Explanations value), the mechanisms by driven factors that lead to changes in risk were explored. Population, elevation and NDVI are the most influential factors leading to changes in risk. Specifically, the increase in risk in the low elevation area is due to the rapid urbanization caused by the increase of population and GDP. While the risk change in higher elevation areas contributes to the variation of vegetation and precipitation. These findings have implications for debris flow mitigation and contribute to the understanding of the multiple factors that impact debris flow risk.

1. Introduction

Debris flow is one of the most destructive types of mass movement (Guo et al., 2024). In the mountainous areas of China, debris flows cause widespread life and economic losses every year (Ding et al., 2016). To decrease the losses caused by debris flows, a wide range of engineering and non-engineering measures were adopted for risk mitigation and prevention. However, in areas with frequent and intense earthquakes like the upper reach of the Min River, earthquake-triggered landslides can provide sufficient loose material for the formation of subsequent debris flow events (Jin et al., 2023). With the rapid urbanization process, debris flows are becoming more frequent in these areas and there is a risk of control and prevention projections failure due to siltation (Huang et al., 2021). Thus, debris flow risk assessment is an important project which can identify the high risk areas and disaster objects of

debris flows (Chen et al., 2021). Based on the risk assessment, identifying the risk dynamic changes can deepen the understanding of the consequences of changes in the human-terrestrial environment. Furthermore, a series of mitigation schedules like urbanization planning, local people migration, dredging of prevention, and control projections can be proposed (Elshorbagy et al., 2017).

To estimate the debris flow risk, there are mainly three methods: numerical simulation methods (Cheng et al., 2022), multi-criteria decision analysis (MCDA)(Chen et al., 2021), and machine learning method (MLM) (Qiu et al., 2024). Up to now, the numerical simulation models for debris flow formation, evolution, and accumulation have been well developed and utilized (Bout et al., 2018; Liu et al., 2021). With the input parameters of sources, channels, and precipitation scenarios, the numerical simulation models can analyze the physical process, hazard area, and other crucial features of debris flows (Cheng et al.,

E-mail address: mingtaoding@swjtu.edu.cn (M. Ding).

^{*} Corresponding author.

2022). However, numerical simulation modeling typically necessitates precise geographical and hydrological data, in addition to a substantial computational burden. It is therefore impractical to undertake numerical modeling efforts at the regional study for all debris flow gullies (Jialei Chen et al., 2021; (Lyu et al., 2019). With this shortage, The MCDA method and machine learning method are widely employed in the regional debris flow risk assessment. The establishment of index system and the weight assignment of indexes are the critical steps of MCDA (Chen et al., 2021). In the earlier studies, methods such as the analytic hierarchy process (AHP), expert scoring method, and fuzzy comprehensive evaluation method are usually used to determine the index weights (Lin et al., 2020). Most of these methods are based on expert experience and knowledge and are highly subjective, which are considered as the limitation of MCDA. (Danumah et al., 2016).

In recent years, the rapid developments of MLMs provide new insight to enhance the efficiency and accuracy of prediction, which have been widely used in risk assessment (Gao et al., 2022). Studies show that Random Forest (RF), Decision Tree (DT), Artificial neural network (ANN), and Support Vector Machine (SVM) are the most widely used algorithms. These algorithms are often applied in an ensemble or hybridized way to analyze most of the flood and landslide events (Zennaro et al., 2021). However, the MLMs usually be seen as a "black box", which cannot describe how parameters and indexes affect the risk (Wang et al., 2024). Thus, the explainable/interpretable models of Shapley additive explanation (SHAP), were proposed to introduce how indicators influence the dependent variable (Bacanin et al., 2024). The SHAP model has been widely used in research, such as the driven factors of runoff and sediment (Bai et al., 2024), the tropical cyclone (Qin et al., 2024), and debris flows (Wang et al., 2024).

In the background of urbanization and climate change, the disaster risk can significantly change in the future (Jiang et al., 2023; Lin et al., 2022). Within the process of urbanization, the debris flow resources can accumulate rapidly due to the slope instability caused by engineering measures (Johnston et al., 2021); (Rohan et al., 2023) . In addition, the increase in population and economy can increase the exposure and vulnerability of debris flows (Cui et al., 2019). Climate change can lead to the variation of hydrothermal conditions and precipitation patterns, which can change the debris flow risk by altering the susceptibility and hazards (Jiang et al., 2023); (Sangelantoni et al., 2018) . Most of these researches are focused on regional study, using the global climate models (GCMs) to evaluate the risk in the future. However, it is still of consideration how the risk changes between the baseline periods and the current periods, due to urbanization and climate change. Accurate identification of current risk variation trends and influencing factors can provide a more accurate projection for the future. Approximately 70 % of China's territory is comprised of mountainous regions, which are home to nearly one-third of the total population (Cui et al., 2022). The southwestern region of China has experienced a number of intense earthquake events, frequent precipitation, extensive human engineering activities, and a significant increase in urbanization (Li et al., 2021; Lin et al., 2022). This provides an ideal setting for the study of the dynamic risk changes and factors driving mechanisms of debris flows.

The primary objectives of this study are: (1) To develop an integrated learning model to assess the debris flow risk in the upper reach of the Min River during the baseline period of 2000 and the current period of 2020; (2) To investigate the dynamic characteristics of risks and compare the changes of disaster bearing body affected by risks; and (3) To analyze the mechanism of indicators of the debris flow risk dynamic changes based on interpretable learning model. This study highlights the changes in the debris flow risk and its influence on the local population and buildings. It also emphasizes the need to consider the impacts of driving differences and changes in factors for regions with different elevations. These efforts can contribute to growing the knowledge of changes in debris flow risk and better local planning and construction.

2. Study area and material

2.1. Study area

The upper reach of the Min River is located in southwestern China, in the transition area between the Tibetan Plateau and the Sichuan Basin (Fig. 1a). The district encompasses an area of 473.76 km², comprising 6 counties and 84 townships. The study area has an azonal arid valley climate, which the mean temperature of the area is 5.7-13.5 °C, and annual precipitation is 400-800 mm of which 80 % is concentrated in the period from May to October (He et al., 2022). The distribution of vegetation cover has clear vertical zonation, which mainly consists of small-leaf, arid shrubs (1300-2200 m), mixed broadleaf-conifer forests, evergreen and deciduous broad-leaved mixed forests (2200-2800 m), Picea and Abies forests (2800–3600 m), and alpine shrubs and meadows (>3600 m) (Shi et al., 2022). A number of strong earthquakes have occurred in the study area, such as the 1933 Diexi Ms 7.5 earthquake, the 1976 Songpan Ms 7.2 earthquake, the 2008 Wenchuan Ms 8.0 earthquake, and the 2017 Jiuzhaigou MS 7.0 earthquake. The active geological activity has resulted in widespread geomorphic landscape and vegetation degradation, and a large number of local accumulations. The climate, vegetation, and geological conditions led to high debris flow activity. Since 2000, there have been 817 debris flow events in the region, with the majority of events occurring in river valleys, as shown in Fig. 1b. Of the 817 documented instances of debris flows, 175 resulted in casualties and economic damage. These events resulted in 35,911 individuals being affected and economic losses amounting to nearly RMB 4 billion. The study area is characterized by extreme differences in altitude, with the lowest point at 727 m elevation and the highest at 5914 m elevation. The debris flow disasters in the study area are distributed over the elevation zone from 800 m to 3600 m, and the distribution statistic is shown in Fig. 1 c. In addition, the population distribution of the study area is also closely related to elevation. Fig. 1 c shows that most of the population is distributed below 2800 m elevation. In addition, between 2000 and 2020, there is a significant increase in the number of people living between 1000—1600 m elevation.

2.2. Data Resource

2.2.1. Debris flow disasters inventory

In this study, the debris flow inventory is collected from the Chengdu Regional Meteorological Center Geological Hazard Forecasting System (CRMCGHFS) (Gao et al., 2022). Under the initiation of CRMCGHFS, we participated in the project of Detailed Risk Investigation of Geological Hazards on Slopes in Sichuan Province. The project identified the current status of geologic hazards (including landslides, mudslides, avalanches, etc.) in each county of Sichuan Province. All the debris flow events in the database were obtained from remote sensing interpretation combined with field investigations. The Investigation process is, firstly, visual interpretation identifies geologic hazards based on remote sensing images (the spatial resolution of remote sensing images is less than 0.5 m). Then, field survey work that includes questionnaires, drones, and other means is conducted to identify the location, the occurrence date, and other attributions of geologic hazards. Finally, the collected data are archived to form a geohazard database. This survey ensured that every debris flow event actually occurred and was recorded at the correct coordinates. The dataset is highly accurate in populated areas; however, it may lack details in areas with minimal human activity. This has minimal impact on the findings presented in this paper.

2.2.2. Debris flows risk conditioning factors

According to the previous study, a total of thirteen factors were selected for the debris flow risk assessment. In order to facilitate differentiation between the aforementioned factors, they have been classified into three distinct categories: trigger factors, subsurface factors, and disaster-bearing factors (Jialei Chen et al., 2021). The trigger factors

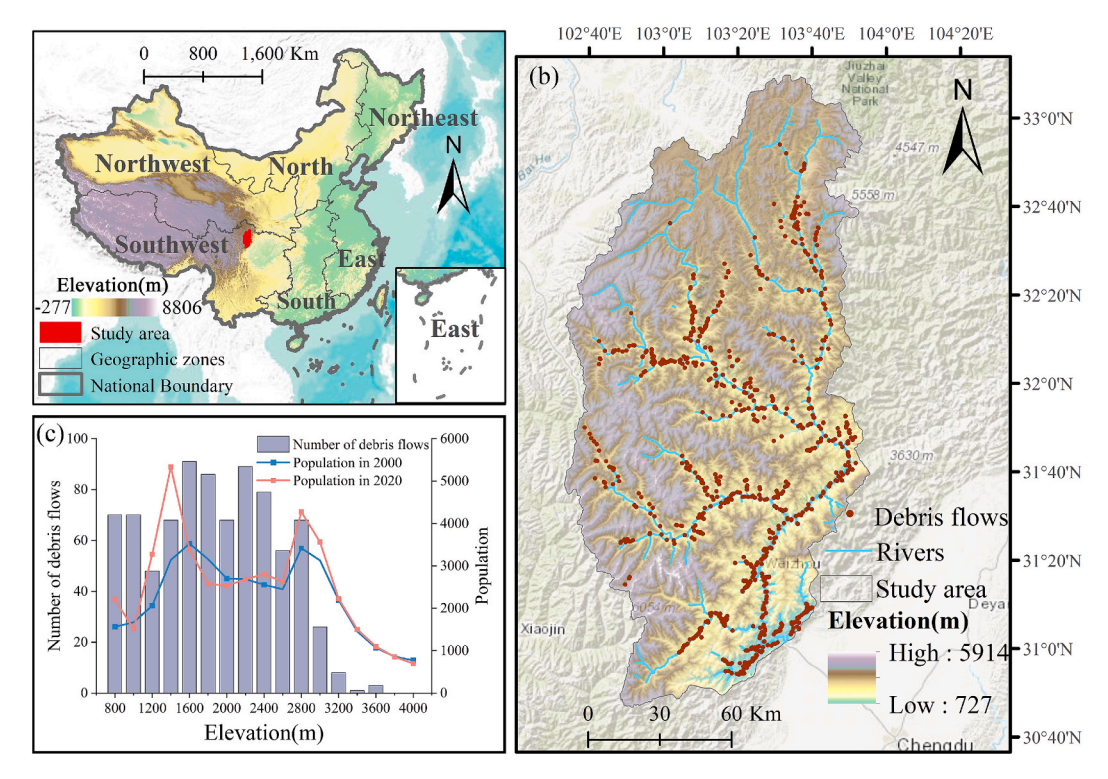


Fig. 1. The basic information about the study area. **c** denotes the distribution of the number of debris flows and the population in each elevation band.

include maximum three-day precipitation (M3DP) and annual precipitation (AP). The subsurface factors include elevation (ELE), slope (SLO), topographic relief (TR), plain curvature (PLC), profile curvature (PRC), melton ratio (MR), the distance to fault (DTF), normalized difference vegetation index (NDVI), and elevation difference (ED). The disasterbearing factors include population counts (POP) and real gross national product (GDP). The spatial distribution of factors is shown in Fig. 2. The MR can be calculated by the formula (Melton, 1966):

$$R_m = \frac{dH}{\sqrt{\Delta}} \tag{1}$$

Where R_m represents the MR value, dH represents the maximum elevation difference (m) within the watershed, A represents the area (m²) of the watershed.

M3DP represents the maximum value of precipitation over a threeday period in a year. It can be used to reflect short periods of heavy precipitation over several days, which can have a significant impact on the triggering of geological disasters (Wu and Chen, 2009). AP is a measure of the overall precipitation conditions and wetness of a given area (Liu et al., 2024). ELE, SLO, TR, PLC, PRC, MR, and ED factors are used to reflect key factors such as debris flow potential, flow direction. and velocity, and are widely employed in the assessment of debris flow hazards (Broeckx et al., 2019; Wang et al., 2024). The presence of active faults can serve as an indicator of the degree of local tectonic activity, thereby providing a potential material source for debris flows. Accordingly, the distance to the fault represents a significant determinant in the assessment of debris flows (Li et al., 2024). NDVI (Chen et al., 2024) has the potential to indicate the growth of local vegetation. This study used the annual average NDVI to measure the overall vegetation for the year. Furthermore, to a certain extent, it can also reflect the activity of landslide material sources (Zhang et al., 2024).

The distributions of five dynamic factors (Fig. 2 i to r) changed significantly between the baseline period and the current periods. The regional average of AP, M3DP, POP, and GDP increased, while NDVI showed a small decrease. The standard deviation (STDev) of AP, NDVI,

POP, and GDP increased, indicating that the dispersion of these factors is increasing. The above changes are in line with what has been found in several literatures that precipitation is increasing, vegetation is declining and population is growing economically in the study area. In addition, the magnitude of the change in NDVI is small, however, in fact, the study area experienced a *Ms* 8.0 magnitude earthquake in 2008 and *Ms* 7.2 magnitude earthquake in 2017, which resulted in significant vegetation attenuation. 2020 When the NDVI of the current period, has been a long-term result of vegetation recovery (See Table 1).

The M3DP and AP were calculated from daily Global Precipitation Measurement database (Huffman et al., 2019), which be validated as accurate for the Sichuan region (Tang et al., 2021). The ELE, SLO, TR, PLC, PRC, RA, and ED were extracted and calculated from the digital elevation model (DEM), which was collected from the Geospatial Data Cloud site, Computer Network Information Center, Chinese Academy of Sciences (GDC, https://www.gscloud.cn/), with a spatial resolution of 90 m \times 90 m. The NDVI data is also obtained from GDC, with a spatial resolution of 1 km \times 1 km. The distribution of fault was obtained from Geocloud, China Geological Survey (geocloud.cgs.gov.cn). Population data was collected from Worldpop. The GDP data is produced by Chen et al (Chen et al., 2021), the detailed information can be found in the study of Chen et al (Jiandong (Chen, 2022). In order to ensure the spatial consistency of the data, a multitude resampling method is used to determine the value of each raster (1 km x 1 km) based on the most frequent value in the raster unit. In addition, the settlement buildings data were collected using Python crawling from Gaode maps, then supplemented and corrected with remote sensing interpretation. The landuse data is produced by Yang and Huang, which can be available for retrieval and querying on Zenedo (Yang and Huang, 2023).

To calculate the risk dynamic change of the study area, we collected the POP, GDP, AP, M3DP, NDVI, and buildings for two periods, 2000 and 2020. The risk in 2000 is used as the baseline period and in 2020 is used as the current period to explore the change in risk.

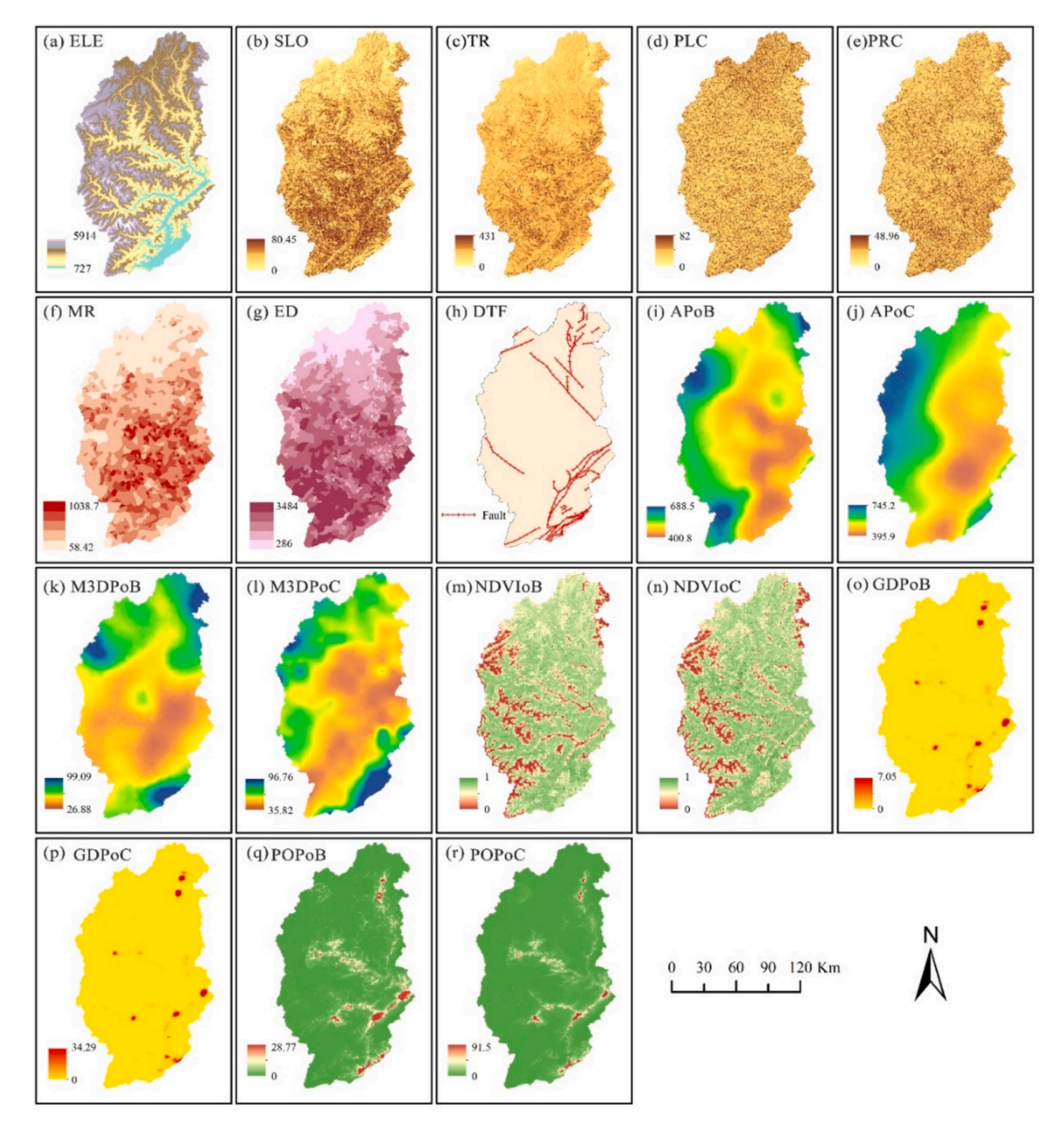


Fig. 2. The spatial pattern and distribution of debris flow risk conditioning factors. (a) elevation, (b) slope, (c) topographic relief, (d) plain curvature, (e) profile curvature, (f) melton ratio, (g) elevation difference, (h) distance to fault, (i) annual precipitation of the baseline period, (j) annual precipitation of the current period, (k) maximum three-day precipitation of the current period, (m) normalized difference vegetation index of the baseline period, (n) normalized difference vegetation index of the current period, (n) normalized difference vegetation index of the baseline period, (n) population of the current period, (n) population of the current period, (n) population of the current period.

3. Methodology

3.1. Debris flow risk estimation modeling

Machine learning models have shown good performance in disaster risk assessment. To estimate the debris flow risk, four learning models were trained and integrated: random forest (RF) (Kim et al., 2018); (Tsagkrasoulis and Montana, 2018), logistic regression (LR) (Ayalew

and Yamagishi, 2005); (Rai et al., 2022); support vector machine (SVM) (Qin et al., 2022; Xiong et al., 2019), and multi-layer perceptron (MLP) (Moayedi et al., 2023; Wang et al., 2021). These models have been widely used in disaster risk assessment and have been shown to have good performance. When performing the modeling, we referenced several other studies to determine the parameters of the model (Wei et al., 2024; Yu et al., 2024). For example, the number of trees for the RF model is n=100, and the maximum depth was set to 10; For MLP, the

Table 1The overview of five dynamic factors.

Indicators name	2000 average	STDev	2020 average	STDev	variation average	STDev
AP (mm)	497.99	54.48	551.25	86.78	53.26	32.3
M3DP (mm)	47.3	11.95	51.84	9.79	4.54	-2.16
NDVI	0.81	0.14	0.79	0.16	-0.02	0.02
POP (person/ km ²)	0.11	0.48	0.13	0.86	0.02	0.38
GDP (10,000 dollars/ km ²)	0.163	0.26	0.43	1.16	0.267	0.9

default architecture consists of one hidden layer with 100 neurons, and the activation function used is 'relu'. The kernel function for SVM is 'rbf', and max_iter for LR model is set to 100. In general, integrated models demonstrate superior evaluation accuracy compared to individual learning models (Lin et al., 2017; Yu, Guo, Jiang, Shao, & Zhou, 2024). In this study, the bagging method was used to integrate four models (Wu et al., 2020). The use of bagging helps to increase model robustness and prevent overfitting by averaging out individual model biases and variances. For modelling training, we generated the same number of non-debris flow points as debris flow events in watersheds without debris flow occurrences (specifically, 177 points). This process was conducted for an equivalent number of non-debris flow events to ensure a balanced and representative sample. Then, 70 % of the 354 events (177 debris flow points and 177 non-debris flow points) were randomly selected as training data, while the remaining 30 % were used as validation data. Based on the training dataset, four models RF, SVM, MLP and LR are trained separately and then they are integrated using bagging. It is important to note that this quantity is based on the period of 2020. Our goal is to develop the most suitable debris flow risk estimation model for 2020, and then retrospectively estimate the risk for 2000. Afterward, based on the established ensemble learning model, the debris flow risks for the two periods in the 1304 catchment units were calculated and validated. In this study, the modeling task is formulated as a regression problem, and the output debris flow risk has a value of [0, 1], with closer to 1 indicating higher risk, means a greater likelihood of debris flow damage occurrence. During the modeling process, hyperparametric optimization is employed to guarantee impartial comparisons between the models. Ultimately, the assessment result is validated through the utilization of debris flow incidents that have resulted in human economic casualties (Jialei Chen et al., 2021). The learning model was constructed in the Python 3.12.2 environment. All subsequent analyses are based on the debris flow risk maps generated by the ensembled model.

3.2. The Shapley Additive Explanations value evaluation

The Shapley Additive Explanation (SHAP) was used to quantify the feature importance to risk (Bai et al., 2024; Qin et al., 2024). SHAP is an emerging technique that has been employed in recent years to gain insight into the modeling process of machine learning and deep learning models (Bacanin et al., 2024). The SHAP is often used in the field of Explainable Artificial Intelligence (XAI) to provide interpretability and transparency in complex model. Furthermore, SHAP is capable of computing interactions between factors by promoting Shapley values, thereby enabling the interpretation of global performance while maintaining local fidelity (Lundberg et al., 2020); (Stojić et al., 2019) . The Shapley value $\phi_i(\nu)$ can be mathematically represented by:

$$\phi_{j}(\nu) = \sum_{S \subseteq \{1,\dots,p\}\{j\}} \frac{|S|!(p-|S|-1)!}{p!} (\nu_{x}(S \cup \{j\}) - \nu_{x}(S))$$
 (2)

Where S is a subset of the p features the model utilizes, and x is the feature value vector of the instance under study. $v_x(S)$ is the forecast for feature values in set S. The calculation of SHAP value be computed and

visualized in the Python 3.12.6, harnessed by the package "shap". The details of SHAP are provided by Wang et al. (Wang et al., 2024).

3.3. Assessment units

The formation of debris flows is most commonly observed in small catchments (Qiao et al., 2021; Qin et al., 2019). Therefore, catchment units are employed as the fundamental unit of assessment for debris flows. Based on DEM and GIS, the study area was divided into 1304 micro catchment units, with the minimum unit is $1.04~\rm km^2$, the maximum unit is $90.70~\rm km^2$. All small catchments are delineated based on ridgelines and valley lines to ensure accuracy. The spatial resolution of the small catchment is consistent with the DEM at $90~\rm m$ x $90~\rm m$, which is a feasible accuracy at the scale of the study area. A total of $68~\rm \%$ of catchment units are less than $20~\rm km^2$ in size, with over $90~\rm \%$ of these units being less than $40~\rm km^2$ in size, and the average area is $17.66~\rm km^2$.

3.4. Accuracy assessment

The receiver operating characteristic (ROC) curve, confusion matrix parameters, overall accuracy, and Kappa coefficient were used to evaluate the performance of the model simulation (Costache and Tien Bui, 2020); (Wei et al., 2024). The area under the curve (AUC) can reflect the accuracy of a model. The value of AUC is between [0,1], with higher values indicating higher model accuracy (Gao and Ding, 2022). ROC is a widely used method to evaluate the performance is disaster assessment. The confusion matrix contains four parameters, true positive (TP), false positive (FP), false negative (FN), and true negative (TN), which were used to characterize the accuracy of the model predictions. Based on these four parameters, accuracy, precision, recall, F1-score, and Kappa coefficient can be calculated. Several metrics are calculated as follows:

$$Accuracy = \frac{TP + TN}{TP + TN + FP + FN} \tag{3}$$

$$Precision = \frac{TP}{TP + FP} \tag{4}$$

$$Recall = \frac{TP}{TP + FN} \tag{5}$$

$$F1 - Score = \frac{2 \times Precision \times Recall}{Precision + Recall}$$
 (6)

$$k = \frac{P_o - P_e}{1 - P_o} \tag{7}$$

The *Accuracy* is the proportion of all samples that the model correctly. The *Precision* refers to the proportion of samples correctly predicted as debris flows out of all the samples predicted to be debris flows by the model. The *Recall* is a metric measuring the model's ability to capture debris flows occurrences. *F1-score* is the harmonic mean of precision and recall, providing a balanced consideration of the model's accuracy and comprehensiveness (Lv et al., 2024). While k is the kappa coefficient, P_o is the observed agreement, and the P_e is the expected agreement.

3.5. Process

Based on ArcGIS, all data underwent pre-processing steps. The values of the indicators were extracted into the watershed units (Xiong et al., 2019). Each indicator was extracted into the watershed units. Specifically, GDP and population were extracted by summing the values of all raster cells within each watershed, while other factors were extracted by calculating the average value of the raster cells within each watershed. The data processing and result analyzing method is shown in Fig. 3. Firstly, the indicator system was divided into two categories: normal and dynamic indexes. The dynamic factors were selected for the periods of

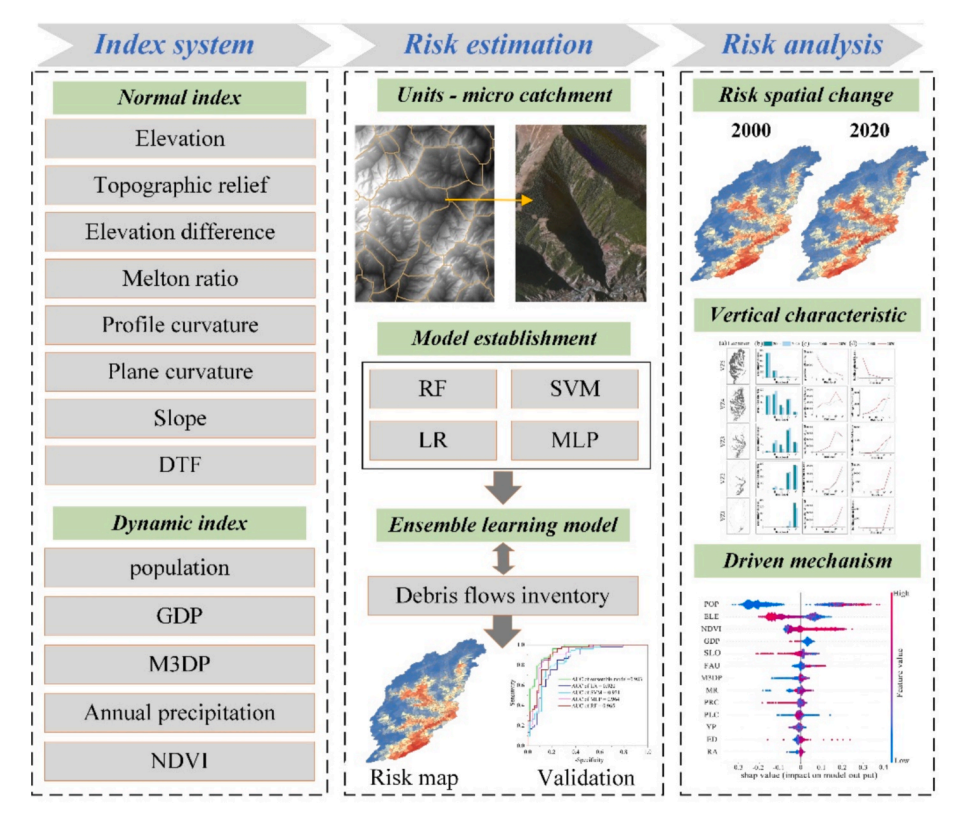


Fig. 3. The process of this study.

2000 and 2020, respectively, resulting in the generation of two datasets. Then, based on the micro catchment units, an ensemble learning model composed of RF, SVM, LR, and MLP was developed for the risk estimation. In this section, the risk maps were output by the ensemble learning model and the accuracy was validated. Finally, the risk spatial–temporal change was analyzed and the vertical characteristics were recognized. The driven factors of the vertical differentiation in risk were identified through the use of SHAP value.

4. Result

4.1. The validation of ROC

The ROC and AUC values of learning models are shown in Fig. 4, where the horizontal coordinate represents the false positive rate, and $\frac{1}{2}$

the vertical coordinate indicates the true positive rate. The ensemble model shows the highest AUC among the models. Higher AUC value indicates better model performance. According to previous study, >0.8 means excellent model performance. Therefore, the AUC value of the ensemble model is 0.983 (in 2020) and 0.976 (in 2000), which means the model has robust fitting and prediction ability (Dodangeh et al., 2020).

Table 2 presents the evaluation metrics for the predicting dataset. From Table 2, it is shown that the ensemble model slightly outperforms other individual models, indicating that the integration of models in this study is effective. Although the ensemble model does not show a clear advantage in some individual metrics, such as the highest Precision (0.89) achieved by the MLP in 2000, it remains the best-performing model overall, consistently maintaining the highest classification accuracy across different scenarios.

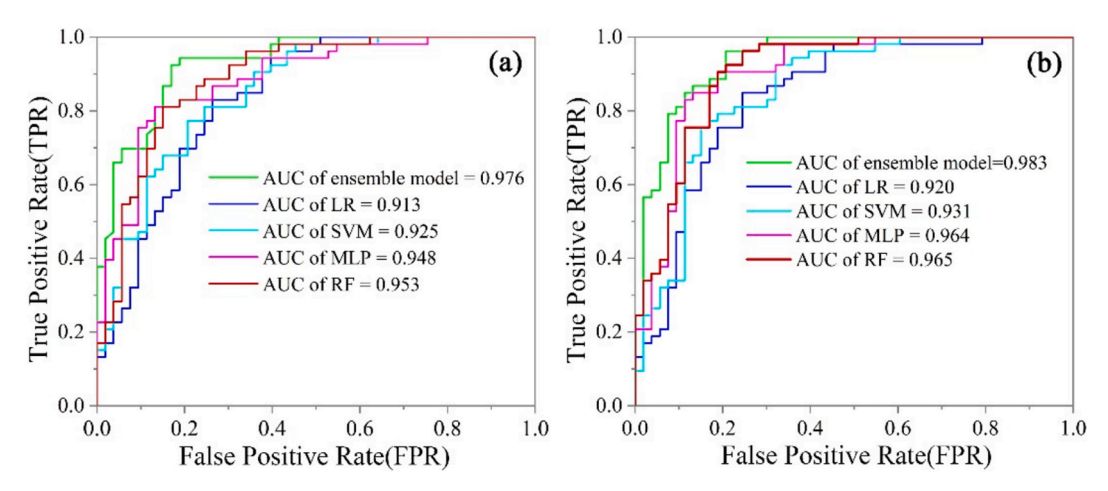


Fig. 4. The ROC of the model. (a) is the validation of 2000. (b) is the validation of 2020.

Table 2 Evaluation of assessment models in two periods.

models Period	Period	Parameters								
		TP	FP	FN	TN	Accuracy	Precision	Recall	F1-score	Карра
RF 20	2000	0.83	0.16	0.17	0.85	0.84	0.83	0.85	0.84	0.68
	2020	0.79	0.21	0.17	0.83	0.81	0.79	0.82	0.81	0.62
LR	2000	0.77	0.23	0.25	0.75	0.76	0.77	0.76	0.77	0.53
	2020	0.81	0.19	0.3	0.7	0.75	0.81	0.73	0.77	0.51
MLP	2000	0.89	0.11	0.23	0.77	0.83	0.89	0.80	0.84	0.66
	2020	0.74	0.26	0.13	0.87	0.80	0.74	0.85	0.79	0.6
	2000	0.74	0.26	0.19	0.81	0.77	0.74	0.80	0.76	0.55
	2020	0.79	0.21	0.23	0.77	0.78	0.79	0.78	0.79	0.57
ensemble model	2000	0.83	0.17	0.11	0.89	0.86	0.83	0.88	0.85	0.72
	2020	0.87	0.13	0.15	0.85	0.86	0.87	0.85	0.86	0.72

4.2. The Spatial-Temporal pattern and change of risk

The equal spacing method was employed to categorize the risk into five classes, namely extremely low (0–0.2), low (0.2–0.4), moderate (0.4–0.6), high (0.6–0.8), and extremely high (0.8–1). Fig. 5 shows the result of debris flow risk assessment. As shown in Fig. 5 (a) and (b), the area with extremely high and high risk is mainly distributed in the southeast and middle regions of the study area. Globally, in 2020 current period, areas with high and extremely high risk encompassed approximately $5000 \, \mathrm{km}^2$, representing 20 percent of the total area. The majority of these regions are situated within river valleys, as well as in the transitional zone between river valleys and high mountainous ranges. The areas with the low and extremely low risk are predominantly situated in the less frequented alpine and sub-alpine regions in the western and northern sections of the study area, taking over an area of 15000 km². (See Table 3).

 Table 3

 The debris risk distribution and change in baseline period and current period.

Risk level	Area(km²) 2000	2020	Risk changes (km²)	Risk change ratio (relative)
Extremely low	11787.80	10940.49	-847.32	−7.19 %
Low	3504.27	4102.43	598.16	17.07 %
Moderate	2652.97	2867.81	214.84	8.1 %
High	2963.30	3383.29	419.99	14.17 %
Extremely high	2124.35	1738.68	-385.67	-18.15 %

Fig. 5 (c) reveals the dynamic pattern of debris flow risk, fluctuations of risk less than 5 % are defined as minor changes. The area with extremely high and extremely low risk is decreased, with the area of $385 \, \mathrm{km}^2$ and $847 \, \mathrm{km}^2$ respectively. The southeastern region of the study area

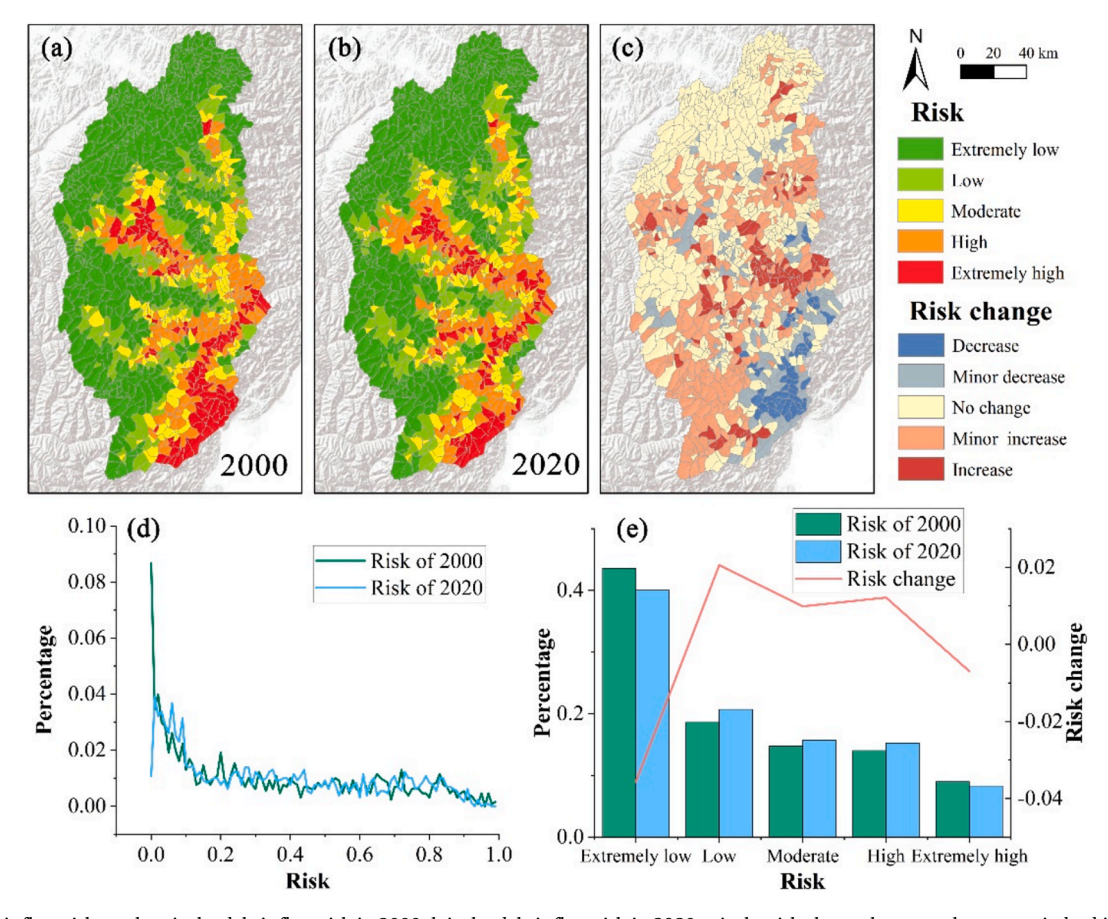


Fig. 5. The debris flow risk result. a is the debris flow risk in 2000, b is the debris flow risk in 2020, c is the risk change between the two periods. d is the trend in the proportion of risk, which is graded at 0.02. e is the proportion of risk in each risk level.

is the primary area exhibiting a decline in risk. The majority of towns in this region has undergone a transition from an extremely high risk grade to a high risk grade. The west-central region of the study area is identified as the area of primary elevated risk. The risk in these areas have undergone a transition, with a shift from moderate-high to high — extremely high risk. Additionally, some low risk areas have been upgraded to moderate. Fig. 5(d) and (e) overview the risk distribution and changes in 2000 and 2020. In the global respective, the risk shows a trend of increase. Locally, extremely high and extremely low risk is decreased, while the other grades are increased. The most significant alterations are occurring in regions with extremely low risk, which are now exhibiting an uptick in risk. In comparison to the baseline period, the extremely high risk area exhibited an 18 % reduction, while the moderate and high risk areas demonstrated an 8 % and 14 % increase, respectively.

4.3. The distribution of risk in vertical zone

The population, economy, and settlements in the upper reach of the Min River have very typical characteristics of vertical zone. Furthermore, according to our assessment result, the debris flow risk distribution exhibits variation across the different vertical zones. According to local government statistics and field surveys, the regions is divided into 5 vertical zones for their different ethnic groups and lifestyles. The vertical zone 1 (VZ1) crosses the elevation of 800–1200 m. The vertical zone 2 (VZ2) crosses the elevation of 1200–2200 m. The vertical zone 3 (VZ3) crosses the elevation of 2200–2800 m. The vertical zone 4 (VZ4) crosses the elevation of 2800–3600 m. The vertical zone 5 (VZ5) has an elevation of over 3600 m. The location of vertical zones, and the overviews of risk in each vertical zone are shown in Fig. 6 and the overviews of risk changes are shown in Table 4.

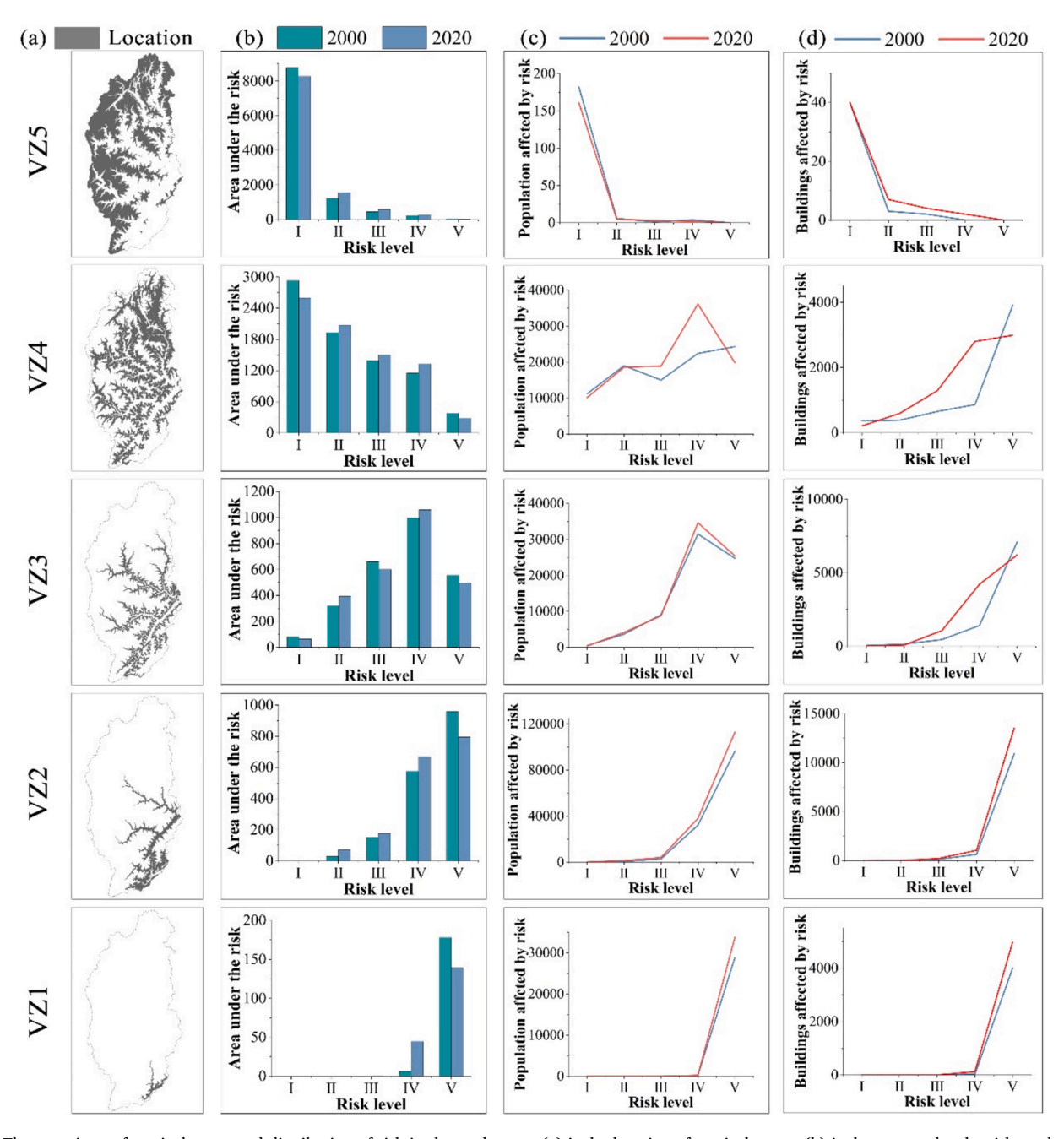


Fig. 6. The overviews of vertical zones and distribution of risk in the study area. (a) is the location of vertical zones. (b) is the area under the risk grades on the vertical zone. (c) is the population affected by the risk. (d) is the buildings affected by the risk.

Table 4The overviews of risk changes in each vertical zone.

Regions	Category	Extremely low	low	moderate	high	Extremely high			
		Relative change rate (%, compared with the baseline period)							
VZ1	Area	0	0	0	20.8 %	-20.8			
	Population	0	0	0	0	14.40			
	buildings	0	0	0	1.94	19.07			
VZ2	Area	0	2.5	1.5	5.5	-9.5			
	Population	0	0.61	0.77	3.81	10.16			
	buildings	0	-0.4	0.5	2.81	17.9			
VZ3	Area	-0.63	2.75	-2.26	2.24	-2.22			
	Population	-0.17	0.66	-0.44	4.27	0.91			
	buildings	-0.39	-0.57	5.22	24.61	-0.77			
VZ4	Area	-4.38	1.80	1.49	2.32	-1.23			
	Population	-1.03	-0.42	3.72	13.25	-4.31			
	buildings	-1.94	2.64	8.11	24.56	-0.12			
VZ5	Area	-4.56	3.19	1.23	0.41	-0.27			
	Population	-12.43	-0.59	1.18	-1.18	0			
	buildings	0	0.784	3.92	0	0			

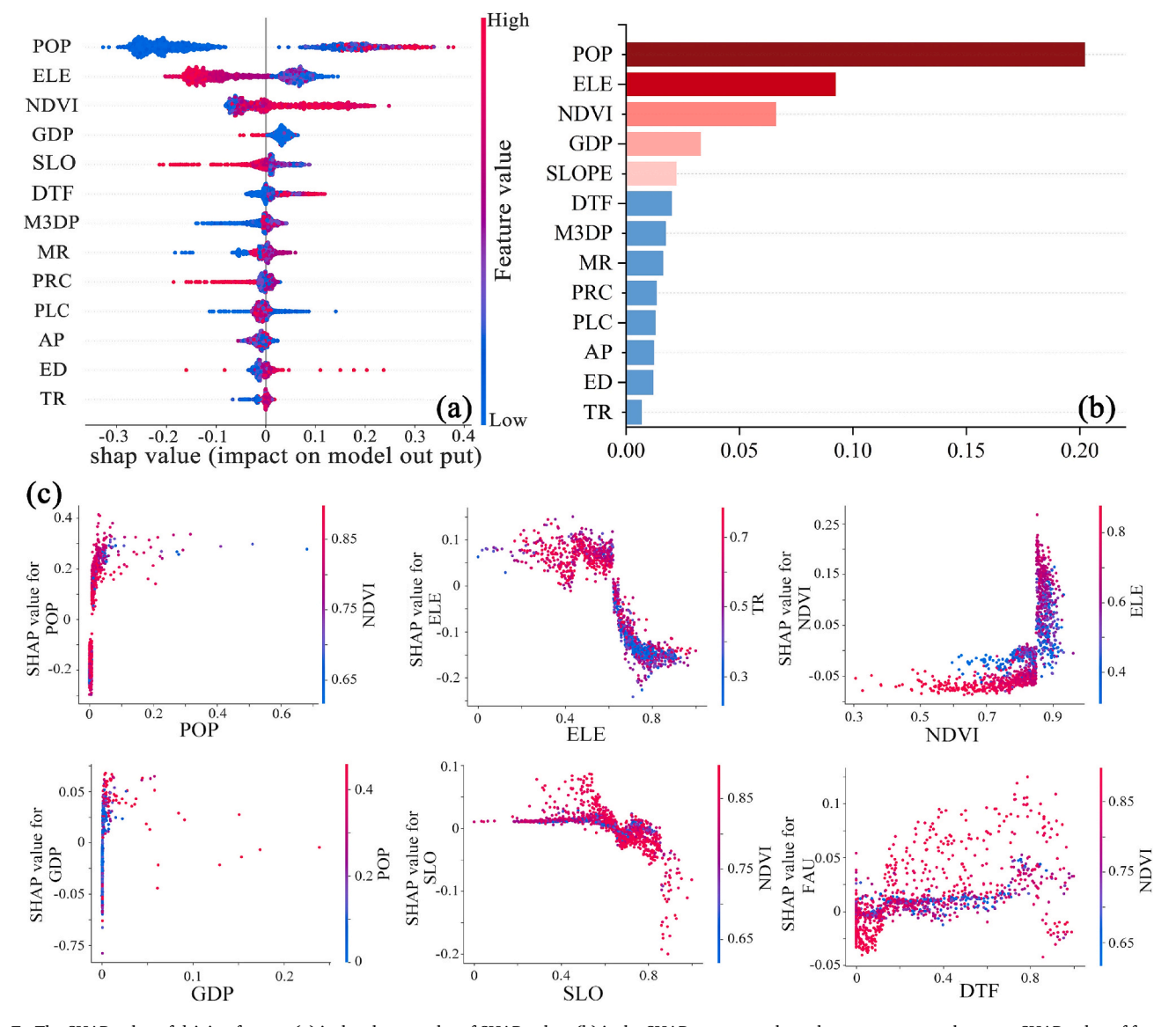


Fig. 7. The SHAP value of driving factors. (a) is the abstract plot of SHAP value. (b) is the SHAP summary plot, where x represents the mean SHAP value of factors, y is the risk conditioning factors. (c) is the dependence plot of the six most important factors.

The extremely high risk area mainly distributed in the VZ1 and VZ2, shows a trend of decrease. Nevertheless, the incidence of high risk area demonstrated an upward trend in all study regions with the exception of VZ5. Low and extremely low risk areas are distributed in VZ4 and VZ5, with a paucity of such areas in other regions. Fig. 6 (c) and (d) shows the number of buildings and populations at risk in each vertical zone. In VZ1 and VZ2, there is a slight increase in the number of people and buildings affected by high and extremely high debris flow risk. The VZ3 and VZ4 regions exhibit the highest diversity of risk grade distribution and the most shifts in risk levels.

4.4. The driven factors and the mechanism of debris flow risk

According to the SHAP-based interpretable machine learning method, the contribution of debris flow risk conditioning factors in each micro catchment to the final risk estimate was analyzed (Fig. 7). Fig. 7 (a) summarizes the contribution of each factor to the debris flows risk in the upper reach of the Min River. Fig. 7 (b) demonstrates that the six factors with the largest SHAP values for debris flow risk are POP, ELE, NDVI, GDP, SLO, and DTF. POP is the most influential factor, with higher POP exerting a positive impact on risk increasing, whereas lower POP exerts a suppressive effect on risk increasing. ELE is the second important factor, with its driving mechanism being the opposite of that of POP. The lower value of ELE has a positive effect on high risk, while an increase in ELE leads to a reduction in risk.

Fig. 7(c) shows the relationship between the six most important factors and debris flow risk SHAP value, with distributions of each factor. As the disaster bearing body, the POP has the most important positive impact on risk increasing. While the NDVI is lower than 0.75, the impact of POP can be transformed more positively. In the areas with low elevation, the increase of TR can lead to the rise of debris flow risk. Whereas at higher elevations, increased TR does not significantly increase risk. In areas of higher elevation, NDVI shows a reducing effect on risk. In areas with elevations of 800–1200, an increase in NDVI leads to an increase in risk. The increase in risk driven by GDP is contingent upon the conjunction of heightened population densities. For SLO and DTF, the effect of them was both significantly affected by the NDVI index.

5. Discussion

5.1. The debris flows risk in the upper reach of the Min River

The upper reach of the Min River is prone to a multitude of geological hazards, particularly in the wake of the Wenchuan 8.0 magnitude earthquake in 2008 (Cui et al., 2011); (Jin et al., 2023). This event has resulted in a proliferation of aftershocks, which have in turn triggered a considerable number of landslides. This has provided a lot of sources for the occurrence of debris flows (Hu et al., 2024). Recent studies have demonstrated that extreme climatic conditions and human engineering activities have served to increase the frequency and severity of debris flow hazards (Deng et al., 2024). From the view of debris flow mitigation, the present study is a necessary contribution. In comparison with other studies, the majority of our high risk areas are situated in locations that exhibit high hazards and vulnerability (Ding et al., 2016; Xiong et al., 2020). With the model's accuracy is 0.976 (2000 baseline period) and 0.983 (2020 current period), we conclude that the evaluation results are reasonable. Along with the aforementioned catastrophe status, the upper reach of the Min River is undergoing a significant process of urbanization, accompanied by an increase in both population and built-up area (Guo et al., 2015). Our assessment results show an upward trajectory in the number of populations and buildings affected by high debris flow risk since the baseline period. In fact, a series of mitigation measures have been carried out by the local government such as construction planning, debris flow control and prevention projections, and population migration policies (Deng et al., 2024). A study demonstrates that local governments in the upper reaches of the Min River have

implemented a multitude of engineering and management measures to mitigate the risk of debris flows, which have been acknowledged by local residents (Deng et al., 2024). The fact that the extremely high risk of debris flows is decreasing is also consistent with our study. In light of the aforementioned changes (Fig. 6 and Tab 3) in population and buildings, which are influenced by debris flow risk, differences in urbanization can be seen in different vertical zones.

Compared to the baseline period, the increase of the buildings in extremely high risk areas are more than the increase in population in the VZ1 and VZ2, suggesting that limited land use is constraining urban expansion. In the areas of VZ3 and VZ4, rapid population and building growth in areas of moderate risk, indicated that it is the area exists a rapid urbanization process. Urbanization can cause an increase in disaster susceptibility and exposure (He et al., 2024; (Strader et al., 2024). Thus, debris flow control and prevention projections are important for risk reduction (Zheng et al., 2022). According to field surveys and previous studies, most debris flow control and prevention projections were precedency constructed in the VZ1 and VZ2, which caused the extremely high risk area to decrease (Deng et al., 2024); (Huang et al., 2021); (Zheng et al., 2022). Whereas the VZ3, VZ4, and VZ5 lack debris flow control, which has increased the risk in these areas. In the future study, we may aim to collect debris flow control and prevention projections data in the area with a view to formulating a comprehensive disaster control strategy. Anyway, based on these findings, the spatial and temporal distribution and variability of debris flow risk were elucidated. Furthermore, the potential influence of population increases and urbanization processes on debris flow risk were indicated.

5.2. Differences in risk change

The upper reach of the Min River can be divided into five distinct vertical zones, each exhibiting a unique risk distribution and change trend. Our results show a decreasing trend in extremely high risk areas but an increase in high risk areas. Nevertheless, in the area between 800 m and 2,200 m, the population and buildings facing exceedingly extremely high risks are on the rise. In the area between 2200 m and 3600 m, with little change in the size of the risk area, the population and buildings impacted by extremely high risk are decrease and the them at medium, and high risk of is increase significantly. This phenomenon can be attributed to the combined effects of climate change, population migration, vegetation evolution, and debris flow prevention and control measures (Deng et al., 2024; Guo et al., 2017). Urbanization has an increasing impact on landslides and other geohazards (Dille et al., 2022). For example, extensive human engineering activities and vegetation degradation can exacerbate geohazard susceptibility and risk (Lin et al., 2022; Zhang et al., 2018).

The combination of the factor's dynamics and the SHAP values provides interesting insights. Fig. 8 shows the summary of five dynamic factors in the baseline period and current period and their SHAP values. Studies have shown that rising population and GDP can lead to increased exposure, in which directly increases risk (Cui et al., 2019); (Rohan et al., 2023). In the vertical zone II region, due to the process of rapid urbanization, both population and GDP show an increasing trend. In this area, the SHAP values for the POP and GDP factors are the highest here, which indicates that urbanization in this region drastically increases the risk (Johnston et al., 2021). Fig. 8(c) indicates the relationship between NDVI with ELE, which the SHAP values increase and then decrease below 0 as elevation increases, and then continue to increase. Some evidence has indicated that the reduction of vegetation can change the alterations in surface and subsurface flow patterns, then increase the geological disaster susceptibility (Yu and Liu, 2015; Zhang et al., 2018). The vegetation of the upper reach of the Min River has been in a degradation trend due to strong earthquakes and urbanization (Guo et al., 2015). From Fig. 7(c) and Fig. 8(c), our findings indicate that the expansion of vegetation in vertical zone IV is increasing the debris flow risk, whereas the heightened risk observed in other vertical zones is

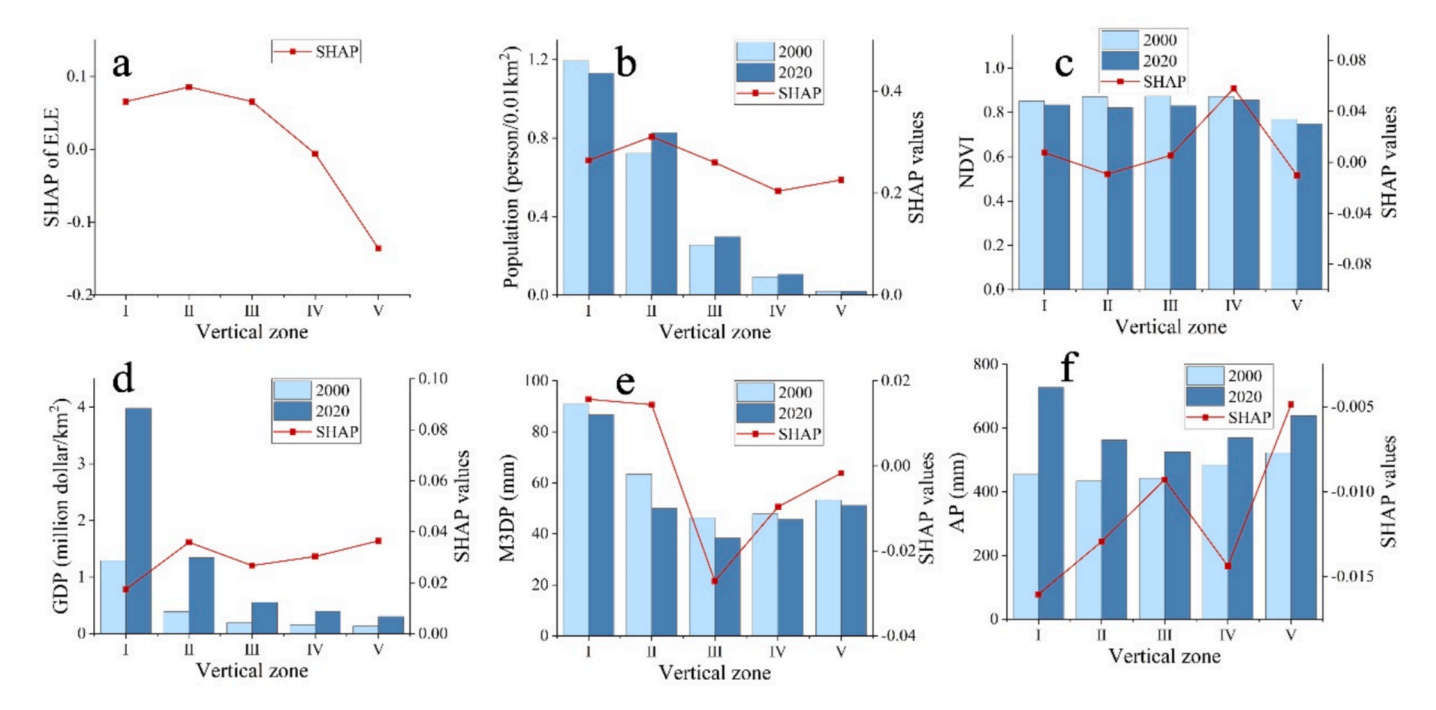


Fig. 8. The temporal change of 5 dynamic factors and their SHAP value in five vertical zones. a is the SHAP of ELE, and b, d, e, f is the POP, NDVI, GDP, M3DP, and AP.

attributed to the degradation of vegetation. We postulate that this phenomenon results from changes in susceptibility due to vegetation degradation. The change in precipitation indicates an overall increase in the precipitation and wetness of the upper reach of the Min River, and the short-term heavy precipitation is decreasing (Fig. 8 e and f). Johnston et al validated that urbanized areas are more sensitive to changes in precipitation than rural areas (Johnston et al., 2021). In our results, the SHAP values of M3DP differ between urbanized and rural areas. In the more urbanized vertical zones I and II, the SHAP values of M3DP are greater than 0, which means the decrease of M3DP contributes to an increased risk. In vertical zones III, IV, and V, which are predominantly mountainous, the reduction in M3DP still gives rise to debris flow risk. This may be attributed to the increase in overall soil moisture due to the up rise of annual precipitation, which has led to a reduction in the precipitation threshold required for debris flow initiation (Cui et al., 2019; He et al., 2024). In such a scenario, the rainfall threshold for debris flow initiation is reached despite a slight decline in the value of M3DP. As can be seen from Fig. 8 e and f, M3DP and AP have a strong impact on debris flow in vertical zones III and IV. These areas are characterized by a considerable number of sources of shattered hills and loose accumulations, which are likely to precipitate the occurrence of debris flow under conditions of uprising humidity (Liu et al., 2017).

5.3. Implications and Limitations

According to our research, the debris flows dynamic risk of the upper reach of the Min River was revealed, and the driven factors of risk in different vertical regions were indicated by using SHAP. Our result shows that the debris flow risk in the upper reach of the Min River is clearly characterized in the vertical zone. The urbanization of vertical zones II and III has exacerbated the local debris flow risk and should focus on risk management. However, the upper reach of Min river is dotted with a larger variety of ethnic groups who have different living customs. For example, ethnic groups in region IV are predominantly agrarian and those in region V are predominantly pastoralist, and information about the impact of their livelihoods and settlements on debris flow risk has not been considered in this paper. In addition, debris

flow basins can be divided into formation, circulation, and accumulation areas, etc. Circulation and accumulation areas are more likely damaged by debris flows. However, this paper does not consider the effect of debris flow disasters in detail. In addition, studies have shown show that cross-validation improves the stability of the model. This study employed a train-test split approach, which lack of cross-validation in model evaluation. In subsequent studies, we expect to develop a physically-based learning model that insightfully discusses the risks and effects of debris flow formation in different regions, while also incorporating cross-validation techniques to enhance model robustness and reliability. Additionally, from a methodological perspective, higher-precision DEMs can provide more accurate indicators and delineate catchment units with greater precision. Therefore, it is recommended to use the highest-possible precision DEM data to minimize errors.

6. Conclusion

In this study, an ensemble learning model composed of random forest, logistic regression, support vector machine, and multi-layer perceptron was constructed to estimate the debris flow risk in the upper reach of the Min River. Then, selecting 5 dynamic factors in the baseline period and the current period, and 9 normal factors, the debris flow risk spatial—temporal patterns over the 20 years were explored. The using of the Shapley Additive Explanations (SHAP) method identified the key factors that lead to the debris flows risk change. Specifically, our findings are:

- (1) The debris flow risk in the upper reach of the Min River is in a trend of increase. The pattern of increased risk is a shift from extremely high risk to high risk in some areas and an overall increase in low and moderate risk.
- (2) Due to the urbanization, despite the area with extremely high risk is decreasing, the population and buildings affected by extremely high risk have still increased. The population and buildings in moderate and low risk areas has increased by 20 % and 30 % respectively.
- (3) The result of SHAP indicates that population, elevation, NDVI, slope, and distance to faults is the most significant factors that contribute to debris flow risk. The relationship between population and

elevation and risk is linear, with population exhibiting a positive correlation with risk and elevation displaying a negative correlation.

(4) The distribution and driven factors of risk vary with elevation. It is imperative to direct particular attention to the processes of urbanization and the debris flow risk management in the vertical zone II and III, in the area with an elevation of 1200–2800 m.

These findings indicate the variability of debris flow risk in the upper reach of the Min River, and can contribute to disaster risk management and urban planning.

CRediT authorship contribution statement

Yufeng He: Writing – review & editing, Writing – original draft, Validation, Software, Methodology, Data curation, Conceptualization. Mingtao Ding: Writing – review & editing, Project administration, Funding acquisition, Data curation. Yu Duan: Writing – review & editing, Validation, Methodology. Hao Zheng: Software, Methodology, Data curation. Wen He: Writing – review & editing, Data curation. Jun Liu: Writing – review & editing, Methodology.

Funding

This study is supported by [1] National Natural Science Foundation of China, Hazard-evolution mechanism of debris flow in different mountain vertical zones settlement areas in the upper reaches of Min River [grant No.42371203]; [2] Sichuan Provincial Science and Technology Department Program Funding, AI-based automatic early warning model and application demonstration of landslide disaster risk along Sichuan-Tibet Railway [grant No. 2025YFHZ0010]; and [3] Science and Technology Program of Aba City, R&D and Demonstration Application of Intelligent Identification and Dynamic Risk Prediction System for Geological Hazards on Mountain Slopes in West Sichuan Province [grant NO. R24YYJSYJ0001]. The authors are grateful to these supports.

Declaration of competing interest

The authors declare that they have no known competing financial interests or personal relationships that could have appeared to influence the work reported in this paper.

Data availability

Data will be made available on request.

References

- Ayalew, L., Yamagishi, H., 2005. The application of GIS-based logistic regression for landslide susceptibility mapping in the Kakuda-Yahiko Mountains. Central Japan. GEOMORPHOLOGY 65 (1), 15–31. https://doi.org/10.1016/j. geomorph.2004.06.010.
- Bacanin, N., Perisic, M., Jovanovic, G., Damaševičius, R., Stanisic, S., Simic, V., Zivkovic, M., Stojic, A., 2024. The explainable potential of coupling hybridized metaheuristics, XGBoost, and SHAP in revealing toluene behavior in the atmosphere. Sci. Total Environ. 929, 172195. https://doi.org/10.1016/j.scitotenv.2024.172195.
- Bai, G., Deng, Y., Chen, M., Zhu, L., Tuo, Y., Nie, M., Zhu, J., Wang, X., 2024. Spatiotemporal evolution of runoff and sediment and their dominant driving factors in the Lower Jinsha River basin. Sci. Total Environ. 951, 175484. https://doi.org/ 10.1016/j.scitotenv.2024.175484.
- Bout, B. v. d. B., Lombardo, L., van Westen, C. J., & Jetten, V. (2018). Integration of two-phase solid fluid equations in a catchment model for flashfloods, debris flows and shallow slope failures. Environmental Modelling & Software, 105, 1-16. doi: 10.1016/j.envsoft.2018.03.017.
- Broeckx, J., Maertens, M., Isabirye, M., Vanmaercke, M., Namazzi, B., Deckers, J., Tamale, J., Jacobs, L., Thiery, W., Kervyn, M., Vranken, L., Poesen, J., 2019. Landslide susceptibility and mobilization rates in the Mount Elgon region. Uganda. Landslides 16 (3), 571–584. https://doi.org/10.1007/s10346-018-1085-y.
- Chen, J., Gao, m., Cheng, S., Hou, W., Song, M., Liu, X., & Liu, Y. (2022). Global $1\ km \times 1\ km$ gridded revised real gross domestic product and electricity consumption during 1992–2019 based on calibrated nighttime light data. Scientific Data, 9(1), 202. doi:10.1038/s41597-022-01322-5.

- Chen, J., Gao, m., Cheng, S., Song, M., Liu, X., & liu, Y. (2021). Global 1 km \times 1 km gridded revised real gross domestic product and electricity consumption during 1992-2019 based on calibrated nighttime light data.
- Chen, J., Huang, G., Chen, W., 2021. Towards better flood risk management: Assessing flood risk and investigating the potential mechanism based on machine learning models. J. Environ. Manage. 293, 112810. https://doi.org/10.1016/j. ienvman.2021.112810.
- Chen, X., Zhang, H., Chen, W., Huang, G., 2021. Urbanization and climate change impacts on future flood risk in the Pearl River Delta under shared socioeconomic pathways. Sci. Total Environ. 762, 143144. https://doi.org/10.1016/j. scitoteny.2020.143144
- Chen, Z., Quan, H., Jin, R., Lin, Z., Jin, G., 2024. Debris flow susceptibility assessment based on boosting ensemble learning techniques: a case study in the Tumen River basin, China. Stoch. Env. Res. Risk A. 38 (6), 2359–2382. https://doi.org/10.1007/s00477-024-02683-6.
- Cheng, H., Huang, Y., Zhang, W., Xu, Q., 2022. Physical process-based runout modeling and hazard assessment of catastrophic debris flow using SPH incorporated with ArcGIS: A case study of the Hongchun gully. Catena 212, 106052. https://doi.org/ 10.1016/j.catena.2022.106052.
- Costache, R., Tien Bui, D., 2020. Identification of areas prone to flash-flood phenomena using multiple-criteria decision-making, bivariate statistics, machine learning and their ensembles. Science of the Total Environment 712, 136492. https://doi.org/10.1016/j.scitotenv.2019.136492.
- Cui, P., 2022. The Landslide/Debris Flow and Control Technology in China. In: Li, R., Napier, T.L., El-Swaify, S.A., Sabir, M., Rienzi, E. (Eds.), Global Degradation of Soil and Water Resources: Regional Assessment and Strategies. Springer Nature Singapore, Singapore, pp. 221–242.
- Cui, P., Chen, X., Zhu, Y., Su, F., Wei, F., Han, Y., Liu, H., Zhuang, J., 2011. The Wenchuan Earthquake (May 12, 2008), Sichuan Province, China, and resulting geohazards. Nat. Hazards 56 (1), 19–36. https://doi.org/10.1007/s11069-009-9392-1.
- Cui, Y., Cheng, D., Choi, C.E., Jin, W., Lei, Y., Kargel, J.S., 2019. The cost of rapid and haphazard urbanization: lessons learned from the Freetown landslide disaster. Landslides 16 (6), 1167–1176. https://doi.org/10.1007/s10346-019-01167-x.
- Danumah, J.H., Odai, S.N., Saley, B.M., Szarzynski, J., Thiel, M., Kwaku, A., Kouame, F., Akpa, L.Y., 2016. Flood risk assessment and mapping in Abidjan district using multicriteria analysis (AHP) model and geoinformation techniques, (cote d'ivoire). Geoenviron. Disasters 3 (1), 10. https://doi.org/10.1186/s40677-016-0044-y.
- Deng, T., Xu, P., Li, M., Lu, Y., Wang, Y., Li, Z., Shravan, K.G., 2024. Socio-scientific quantification of the comprehensive benefits of debris flow mitigation measures for villages in western Sichuan. China. Journal of Mountain Science 21 (5), 1598–1612. https://doi.org/10.1007/s11629-023-8397-7.
- Dille, A., Dewitte, O., Handwerger, A.L., d'Oreye, N., Derauw, D., Ganza Bamulezi, G., Ilombe Mawe, G., Michellier, C., Moeyersons, J., Monsieurs, E., Mugaruka Bibentyo, T., Samsonov, S., Smets, B., Kervyn, M., Kervyn, F., 2022. Acceleration of a large deep-seated tropical landslide due to urbanization feedbacks. Nat. Geosci. 15 (12), 1048–1055. https://doi.org/10.1038/s41561-022-01073-3.
- Ding, M., Heiser, M., Hübl, J., Fuchs, S., 2016. Regional vulnerability assessment for debris flows in China—a CWS approach. Landslides 13 (3), 537–550. https://doi. org/10.1007/s10346-015-0578-1.
- Dodangeh, E., Choubin, B., Eigdir, A.N., Nabipour, N., Panahi, M., Shamshirband, S., Mosavi, A., 2020. Integrated machine learning methods with resampling algorithms for flood susceptibility prediction. Sci. Total Environ. 705, 135983. https://doi.org/ 10.1016/j.scitotenv.2019.135983.
- Elshorbagy, A., Bharath, R., Lakhanpal, A., Ceola, S., Montanari, A., Lindenschmidt, K.E., 2017. Topography- and nightlight-based national flood risk assessment in Canada. Hydrol. Earth Syst. Sci., 21 (4), 2219–2232. https://doi.org/10.5194/hess-21-2219-2017
- Gao, Z., Ding, M., 2022. Application of convolutional neural network fused with machine learning modeling framework for geospatial comparative analysis of landslide susceptibility. Nat. Hazards 113 (2), 833–858. https://doi.org/10.1007/s11069-022.05326-7
- Gao, Z., Ding, M., Huang, T., Liu, X., Hao, Z., Hu, X., Chuanjie, X., 2022. Landslide risk assessment of high-mountain settlements using Gaussian process classification combined with improved weight-based generalized objective function. Int. J. Disaster Risk Reduct. 67, 102662. https://doi.org/10.1016/j.ijdrr.2021.102662.
- Guo, X., Hürlimann, M., Cui, P., Chen, X., Li, Y., 2024. Monitoring cases of rainfall-induced debris flows in China. Landslides 21 (10), 2447–2466. https://doi.org/10.1007/s10346-024-02316-7.
- Guo, Y.-L., Wang, Q., Yan, W.-P., Zhou, Q., Shi, M.-Q., 2015. Assessment of habitat suitability in the Upper Reaches of the Min River in China. J. Mt. Sci. 12 (3), 737–746. https://doi.org/10.1007/s11629-013-2662-0.
- Guo, Y., Wang, Q., Fan, M., 2017. Exploring the Relationship between the Arid Valley Boundary's Displacement and Climate Change during 1999–2013 in the Upper Reaches of the Min River. China. ISPRS International Journal of Geo-Information 6 (5) 146.
- He, K., Chen, X., Yu, X., Dong, C., Zhao, D., 2024. Evaluation and prediction of compound geohazards in highly urbanized regions across China's Greater Bay Area. J. Clean. Prod. 449, 141641. https://doi.org/10.1016/j.jclepro.2024.141641.
- He, K., Chen, X., Zhao, D., Yu, X., Jin, Y., Liang, Y., 2024. Precipitation-induced landslide risk escalation in China's urbanization with high-resolution soil moisture and multisource precipitation product. J. Hydrol. 638, 131536. https://doi.org/10.1016/j. ibudeal 2024.131526
- He, Y., Ding, M., Liu, K., Lei, M., 2022. The Impact of Geohazards on Sustainable Development of Rural Mountain Areas in the Upper Reaches of the Min River. Front. Earth Sci. 10, 1–11. https://doi.org/10.3389/feart.2022.862544.

- Hu, X., Wang, J., Hu, J., Hu, K., Zhou, L., Liu, W., 2024. Probabilistic identification of debris flow source areas in the Wenchuan earthquake-affected region of China based on Bayesian geomorphology. Environ. Earth Sci. 83 (18), 528. https://doi.org/ 10.1007/s12665-024-11833-6.
- Huang, T., Ding, M., Gao, Z., Téllez, R.D., 2021. Check dam storage capacity calculation based on high-resolution topogrammetry: Case study of the Cutou Gully, Wenchuan County. China. Science of the Total Environment 790, 148083. https://doi.org/ 10.1016/j.scitoteny.2021.148083.
- Huffman, G., Stocker, E., Bolvin, D., Nelkin, E., & Jackson, T. (2019). GPM IMERG Early Precipitation L3 1 day 0.1 degree x 0.1 degree V06.
- Jiang, R., Lu, H., Yang, K., Chen, D., Zhou, J., Yamazaki, D., Pan, M., Li, W., Xu, N., Yang, Y., Guan, D., Tian, F., 2023. Substantial increase in future fluvial flood risk projected in China's major urban agglomerations. Commun. Earth Environ. 4 (1), 389. https://doi.org/10.1038/s43247-023-01049-0.
- Jin, W., Cui, P., Zhang, G., Wang, J., Zhang, Y., Zhang, P., 2023. Evaluating the post-earthquake landslides sediment supply capacity for debris flows. Catena 220 (PartA), 106649. https://doi.org/10.1016/j.catena.2022.106649.
- Johnston, E.C., Davenport, F.V., Wang, L., Caers, J.K., Muthukrishnan, S., Burke, M., Diffenbaugh, N.S., 2021. Quantifying the Effect of Precipitation on Landslide Hazard in Urbanized and Non-Urbanized Areas. Geophys. Res. Lett. 48 (16), e2021GL094038. https://doi.org/10.1029/2021GL094038.
- Kim, J.-C., Lee, S., Jung, H.-S., Lee, S., 2018. Landslide susceptibility mapping using random forest and boosted tree models in Pyeong-Chang. Korea. Geocarto International 33 (9), 1000–1015. https://doi.org/10.1080/ 10106049.2017.1323964.
- Li, G., Cao, H., 2021. Urbanization in China. In: Li, G., Cao, H. (Eds.), Understanding Spatial-Temporal Patterns of the Ethnic Minority Mobility in China's Urbanization. Springer Singapore, Singapore, pp. 5–27.
- Li, Y., Jiang, W., Feng, X., LV, S., Yu, W., Ma, E., 2024. Debris flow susceptibility mapping in alpine canyon region: a case study of Nujiang Prefecture. Bulletin of Engineering Geology and the Environment 83 (5), 169. https://doi.org/10.1007/s10064-024-03657-2
- Lin, G.-F., Chang, M.-J., Huang, Y.-C., Ho, J.-Y., 2017. Assessment of susceptibility to rainfall-induced landslides using improved self-organizing linear output map, support vector machine, and logistic regression. Eng. Geol. 224, 62–74. https://doi. org/10.1016/j.enggeo.2017.05.009.
- Lin, K., Chen, H., Xu, C.-Y., Yan, P., Lan, T., Liu, Z., Dong, C., 2020. Assessment of flash flood risk based on improved analytic hierarchy process method and integrated maximum likelihood clustering algorithm. J. Hydrol. 584, 124696. https://doi.org/ 10.1016/j.ihydrol.2020.124696.
- Lin, Q., Steger, S., Pittore, M., Zhang, J., Wang, L., Jiang, T., Wang, Y., 2022. Evaluation of potential changes in landslide susceptibility and landslide occurrence frequency in China under climate change. Science of the Total Environment 850, 158049. https:// doi.org/10.1016/i.scitoteny.2022.158049.
- Liu, Q., Cheng, W., Sun, D., Wang, N., Fang, Y., 2017. Distribution Characteristics of Historical Mountain Flood in China. Journal of Geo-Information Science 19 (12), 1557–1566. In Chineses.
- Liu, S., Liu, S., Lv, D., Wei, L., Ao, M., Pan, X., Li, B., Cui, Y., Wang, L., He, X., 2024. Debris flow susceptibility and hazard assessment in Fushun based on hydrological response units. Nat. Hazards 120 (9), 8667–8693. https://doi.org/10.1007/s11069-024_06544_v
- Liu, W., Yang, Z., He, S., 2021. Modeling the landslide-generated debris flow from formation to propagation and run-out by considering the effect of vegetation. Landslides 18 (1), 43–58. https://doi.org/10.1007/s10346-020-01478-4.
- Lundberg, S.M., Erion, G., Chen, H., DeGrave, A., Prutkin, J.M., Nair, B., Katz, R., Himmelfarb, J., Bansal, N., Lee, S.-I., 2020. From local explanations to global understanding with explainable AI for trees. Nat. Mach. Intell. 2 (1), 56–67. https:// doi.org/10.1038/s42256-019-0138-9.
- Lv, J., Zhang, R., Shama, A., Hong, R., He, X., Wu, R., Bao, X., Liu, G., 2024. Exploring the spatial patterns of landslide susceptibility assessment using interpretable Shapley method: Mechanisms of landslide formation in the Sichuan-Tibet region. J. Environ. Manage. 366, 121921. https://doi.org/10.1016/j.jenvman.2024.121921.
- Lyu, H.M., Shen, S.L., Yang, J., Yin, Z.Y., 2019. Inundation analysis of metro systems with the storm water management model incorporated into a geographical information system: a case study in Shanghai. Hydrol. Earth Syst. Sci., 23 (10), 4293–4307. https://doi.org/10.5194/hess-23-4293-2019.
- Melton, M.A., 1966. The Geomorphic and Paleoclimatic Significance of Alluvial Deposits in Southern Arizona: A Reply. J. Geol. 74 (1), 102–106. https://doi.org/10.1086/ 627147
- Moayedi, H., Canatalay, P.J., Ahmadi Dehrashid, A., Cifci, M.A., Salari, M., Le, B.N., 2023. Multilayer Perceptron and Their Comparison with Two Nature-Inspired Hybrid Techniques of Biogeography-Based Optimization (BBO) and Backtracking Search Algorithm (BSA) for Assessment of Landslide Susceptibility. Land 12 (1), 242.
- Qiao, S., Qin, S., Sun, J., Che, W., Yao, J., Su, G., Chen, Y., Nnanwuba, U., 2021.

 Development of a region-partitioning method for debris flow susceptibility mapping.

 J. Mt. Sci. 18 (5), 1177–1191. https://doi.org/10.1007/s11629-020-6497-1.
- Qin, L., Zhu, L., Liu, B., Li, Z., Tian, Y., Mitchell, G., Shen, S., Xu, W., Chen, J., 2024. Global expansion of tropical cyclone precipitation footprint. Nat. Commun. 15 (1), 4824. https://doi.org/10.1038/s41467-024-49115-1.
- Qin, S., Lv, J., Cao, C., Ma, Z., Hu, X., Liu, F., Qiao, S., Dou, Q., 2019. Mapping debris flow susceptibility based on watershed unit and grid cell unit: a comparison study. Geomat. Nat. Haz. Risk 10 (1), 1648–1666. https://doi.org/10.1080/ 19475705.2019.1604572.
- Qin, S., Qiao, S., Yao, J., Zhang, L., Liu, X., Guo, X., Chen, Y., Sun, J., 2022. Establishing a GIS-based evaluation method considering spatial heterogeneity for debris flow

- susceptibility mapping at the regional scale. Nat. Hazards 114 (3), 2709–2738. https://doi.org/10.1007/s11069-022-05487-5.
- Qiu, C., Su, L., Pasuto, A., Bossi, G., Geng, X., 2024. Economic Risk Assessment of Future Debris Flows by Machine Learning Method. International Journal of Disaster Risk Science 15 (1), 149–164. https://doi.org/10.1007/s13753-024-00545-x.
- Rai, D.K., Xiong, D., Zhao, W., Zhao, D., Zhang, B., Dahal, N.M., Wu, Y., Baig, M., 2022. An Investigation of Landslide Susceptibility Using Logistic Regression and Statistical Index Methods in Dailekh District. Nepal. Chinese Geographical Science 32 (5), 834–851. https://doi.org/10.1007/s11769-022-1304-2.
- Rohan, T., Shelef, E., Mirus, B., Coleman, T., 2023. Prolonged influence of urbanization on landslide susceptibility. Landslides 20 (7), 1433–1447. https://doi.org/10.1007/s10346-023-02050-6
- Sangelantoni, L., Gioia, E., Marincioni, F., 2018. Impact of climate change on landslides frequency: the Esino river basin case study (Central Italy). Nat. Hazards 93 (2), 849–884. https://doi.org/10.1007/s11069-018-3328-6.
- Shi, W., Jiang, H., Xu, H., Ma, S., Fan, J., Zhang, S., Guo, Q., Wei, X., 2022. Response of modern fluvial sediments to regional tectonic activity along the upper Min River, eastern Tibet. Earth Surf. Dynam., 10 (6), 1195–1209. https://doi.org/10.5194/ esurf.10.1195.2022
- Stojić, A., Stanić, N., Vuković, G., Stanišić, S., Perišić, M., Šoštarić, A., Lazić, L., 2019. Explainable extreme gradient boosting tree-based prediction of toluene, ethylbenzene and xylene wet deposition. Sci. Total Environ. 653, 140–147. https://doi.org/10.1016/j.scitotenv.2018.10.368.
- Strader, S.M., Gensini, V.A., Ashley, W.S., Wagner, A.N., 2024. Changes in tornado risk and societal vulnerability leading to greater tornado impact potential. npj. Nat. Hazards 1 (1), 20. https://doi.org/10.1038/s44304-024-00019-6.
- Tang.Shunxian, Rui, L., & Jianxin, H. (2021). Modeling and Evaluating Systematic and Random Errors in Multiscale GPM IMERG Summer Precipitation Estimates Over the Sichuan Basin. IEEE Journal of Selected Topics in Applied Earth Observations and Remote Sensing, 14, 4709-4719. doi:10.1109/JSTARS.2021.3076197.
- Tsagkrasoulis, D., Montana, G., 2018. Random forest regression for manifold-valued responses. Pattern Recogn. Lett. 101, 6–13. https://doi.org/10.1016/j. patrec.2017.11.008.
- Wang, N., Zhang, H., Dahal, A., Cheng, W., Zhao, M., Lombardo, L., 2024. On the use of explainable AI for susceptibility modeling: Examining the spatial pattern of SHAP values. Geosci. Front. 15 (4), 101800. https://doi.org/10.1016/j.gsf.2024.101800.
- Wang, Q., Wang, C., Tang, H., Wu, D., Wang, F., 2024. Semi-supervised deep learning based on label propagation algorithm for debris flow susceptibility assessment in few-label scenarios. Stoch. Env. Res. Risk A. 38 (7), 2875–2890. https://doi.org/ 10.1007/s00477-024-02719-x.
- Wang, Y., Fang, Z., Hong, H., Costache, R., Tang, X., 2021. Flood susceptibility mapping by integrating frequency ratio and index of entropy with multilayer perceptron and classification and regression tree. J. Environ. Manage. 289, 112449. https://doi.org/ 10.1016/i.jenyman.2021.112449.
- Wei, Y., Qiu, H., Liu, Z., Huangfu, W., Zhu, Y., Liu, Y., Yang, D., Kamp, U., 2024. Refined and dynamic susceptibility assessment of landslides using InSAR and machine learning models. Geosci. Front. 15 (6), 101890. https://doi.org/10.1016/j.
- Wu, C.-H., Chen, S.-C., 2009. Determining landslide susceptibility in Central Taiwan from rainfall and six site factors using the analytical hierarchy process method. Geomorphology 112 (3), 190–204. https://doi.org/10.1016/j. geomorph.2009.06.002.
- Wu, Y., Ke, Y., Chen, Z., Liang, S., Zhao, H., Hong, H., 2020. Application of alternating decision tree with AdaBoost and bagging ensembles for landslide susceptibility mapping. Catena 187, 104396. https://doi.org/10.1016/j.catena.2019.104396.
- Xiong, J., Li, J., Cheng, W., Wang, N., Guo, L., 2019. A GIS-Based Support Vector Machine Model for Flash Flood Vulnerability Assessment and Mapping in China. ISPRS Int. J. Geo Inf. 8 (7), 297.
- Xiong, K., Adhikari, B.R., Stamatopoulos, C.A., Zhan, Y., Wu, S., Dong, Z., Di, B., 2020.Comparison of Different Machine Learning Methods for Debris Flow SusceptibilityMapping: A Case Study in the Sichuan Province. China. Remote Sensing 12 (2), 295.
- Yang, J., & Huang, X. (2023). The 30 m annual land cover datasets and its dynamics in China from 1985 to 2022.
- Yu, L., Wang, Y., Pradhan, B., 2024. Enhancing landslide susceptibility mapping incorporating landslide typology via stacking ensemble machine learning in Three Gorges Reservoir. China. Geoscience Frontiers 15 (4), 101802. https://doi.org/ 10.1016/j.gsf.2024.101802.
- Yu, M., Liu, Y., 2015. The possible impact of urbanization on a heavy rainfall event in Beijing. J. Geophys. Res. Atmos. 120 (16), 8132–8143. https://doi.org/10.1002/ 2015 D003336
- Yu, R., Guo, R., Jiang, L., Shao, Y., Zhou, Z., 2024. Susceptibility assessment of glacier-related debris flow on the southeastern Tibetan Plateau using different hybrid machine learning models. Sci. Total Environ. 954, 176400. https://doi.org/10.1016/j.scitoteny.2024.176400.
- Zennaro, F., Furlan, E., Simeoni, C., Torresan, S., Aslan, S., Critto, A., Marcomini, A., 2021. Exploring machine learning potential for climate change risk assessment. Earth Sci. Rev. 220, 103752. https://doi.org/10.1016/j.earscirev.2021.103752.

- Zhang, W., Villarini, G., Vecchi, G.A., Smith, J.A., 2018. Urbanization exacerbated the rainfall and flooding caused by hurricane Harvey in Houston. Nature 563 (7731), 384–388. https://doi.org/10.1038/s41586-018-0676-z
- 384–388. https://doi.org/10.1038/s41586-018-0676-z.
 Zhang, X., Tang, C., Tie, Y., Li, X., Tang, C., Xiong, J., Chen, M., Gong, L., 2024. Dynamic susceptibility assessment of debris flow hazard after a strong earthquake, Wenchuan
- County, Sichuan, China. Landslides 21 (8), 1915–1928. https://doi.org/10.1007/s10346-024-02246-4.
- Zheng, H., Ding, M., Huang, T., Gao, Z., 2022. Benefit evaluation of geotechnical projects for debris flow prevention and control based on projection pursuit in Wenchuan County, SW China. J. Earth Sci. 1–24.